Inference of Soil Freezing Front Depth During the Freezing Period From the *L*-Band Passive Microwave Brightness Temperature

Shaoning Lv, Lianyu Yu, Yijian Zeng, Jun Wen, Clemens Simmer, and Zhongbo Su

***Abstract*—The freezing front depth (z_{ff}) of annual freeze–thaw cycles is critical for monitoring the dynamics of the cryosphere under climate change because z_{ff} is a sensitive indicator of the heat balance over the atmosphere-cryosphere interface. Meanwhile, although it is very promising for acquiring global soil moisture distribution, the *L*-band microwave remote sensing products over seasonally frozen grounds and permafrost is much less than in wet soil. This study develops an algorithm, i.e., the brightness temperature inferred freezing front (BT-FF) model, for retrieving the interannual z_{ff} with the diurnal amplitude variation of *L*-band brightness temperature (ΔT_B) during the freezing period. The new algorithm assumes first, the daily-scale solar radiation heating/cooling effect causes the daily surface thawing depth (z_{tf}) variation, which leads further to ΔT_B; second, ΔT_B can be captured by an *L*-band radiometer; third, z_{tf} and z_{ff} are negatively linear correlated and their relation can be quantified using the Stefan equation. In this study, the modeled soil temperature profiles from the land surface model (STEMMUS-FT, i.e., simultaneous transfer of energy, mass, and momentum in unsaturated soil with freeze and thaw) and T_B observations from a tower-based *L*-band radiometer (ELBARA-III) at Maqu are used to validate the BT-FF model. It shows that, first, ΔT_B can be precisely estimated from z_{tf} during the daytime; second, the decreasing of z_{tf} is linearly related to the increase of z_{ff} with the Stefan equation; third, the accuracy of retrieved z_{ff} is about 5–25 cm; fourth, the proposed model is applicable during the freezing period. The study is expected to extend the application of *L*-band T_B data in cryosphere/meteorology and construct global freezing depth dataset in the future.**

***Index Terms*—Diurnal amplitude variation (DAV), freezing front, *L*-band, passive microwave remote sensing.**

Manuscript received 2 September 2022; revised 17 December 2022; accepted 30 January 2023. Date of publication 3 February 2023; date of current version 2 May 2023. This work was supported in part by the National Natural Science Foundation of China under Grant 42075150, in part by the Natural Science Foundation of Shanghai under Grant 21ZR1405500, in part by the Deutsche Forschungsgemeinschaft via the Research Group FOR2131 on "Data Assimilation for Improved Characterization of Fluxes across Compartmental Interfaces," subproject P2, in part by the ESA MOST Dragon IV Program (Monitoring Water and Energy Cycles at Climate Scale in the Third Pole Environment), and in part by The Netherlands Organization for Scientific Research under Grant ALW-GO/14–29. *(Corresponding author: Jun Wen.)*

Shaoning Lv is with the Department of Atmospheric and Oceanic Sciences and Institute of Atmospheric Sciences, Fudan University, Shanghai 200438, China, and also with the Zhuhai Fudan Innovation Research Institute, Zhuhai 519000, China (e-mail: lvshaoning@fudan.edu.cn).

Lianyu Yu, Yijian Zeng, and Zhongbo Su are with the Department of Water Resources, Faculty of Geo-information Science and Earth Observation (ITC), University of Twente, 7500AE Enschede, The Netherlands (e-mail: l.yu@utwente.n; y.zeng@utwente.nl; z.su@utwente.nl).

Jun Wen is with the Plateau Atmosphere and Environment Key Laboratory of Sichuan Province, Chengdu University of Information Technology, Chengdu 610225, China (e-mail: jwen@cuit.edu.cn).

Clemens Simmer is with the Institute for Geosciences—Meteorology, University of Bonn, 53121 Bonn, Germany (e-mail: csimmer@uni-bonn.de).

Digital Object Identifier 10.1109/JSTARS.2023.3241876

I. Introduction

Approximately 56% of topsoil in the northern hemisphere's landmass freezes at least for some time each year, including permafrost, which accounts for about 24% relatively [1]. Unlike permafrost in deeper soil depths, the soil freeze–thaw (FT) occurs at depths of centimeters to meters, drastically altering water and energy exchange between the land surface and the atmosphere [2], [3], [4]. In this term, the FT state transition refers to seasonal albedo changes that firmly shift the radiation balance over the land [5], [6], [7]. Besides albedo, the latent/sensible heat fluxes affected by FT have considerable changes at diurnal scales and impact the soil's water and energy states in the upper few centimeters [8], [9], [10], [11], [12], [13], [14]. Thus, FT state monitoring is sensitive and critical to weather prediction, climate forecasting, hydrology, and agriculture [15], [16]. However, due to high expense and poor representativeness, FT state monitoring is hard to achieve by regular measurements at in situ. On the other hand, the FT states are also critical to the forward modeling of microwave signals [17], [18], [19], [20], [21], which can be further applied to studies about land-atmosphere interactions with data assimilation [22], [23].

Since the launch of Skylab in the 1970s [24], passive remote sensing of the land surface condition, including FT state in microwave frequencies, has become a promising tool. Studies on the FT state detection started with shorter microwave bands, such as the Nimbus-7 Scanning Multichannel Microwave Radiometer SMMR [25], the Special Sensor Microwave/Imager SSM/I [26], and the Advanced Microwave Scanning Radiometer for EOS AMSR-E [27].

With a deeper penetration depth than previous microwave bands used by the Advanced Microwave Scanning Radiometer 2 (AMSRe/AMSR2) [28], Funyun-3 [29], and Advanced Scatterometer (ASCAT) [30], *L*-band microwaves have developed various FT states retrieving algorithms [31], [32], [33], [34]. Besides polarization [35], [36], single-channel [37], and multichannel [38] algorithms, the diurnal amplitude variation (DAV) of brightness temperature (T_B) has been used to detect snow and ice with higher microwave frequencies [34], [39], [40], [41], [42], but not yet for the *L*-band. At the *L*-band, ΔT_B (i.e., DAV of T_B hereafter) induced by freezing/thawing (ca. 100 K)

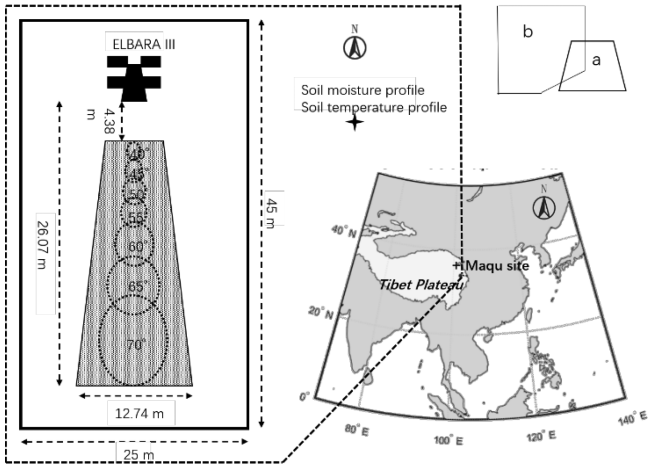

Fig. 1. (a) Location of the maqu experiment on the Tibetan plateau. (b) Illustration of the footprint observed by ELBARA-III (circles with small dots).

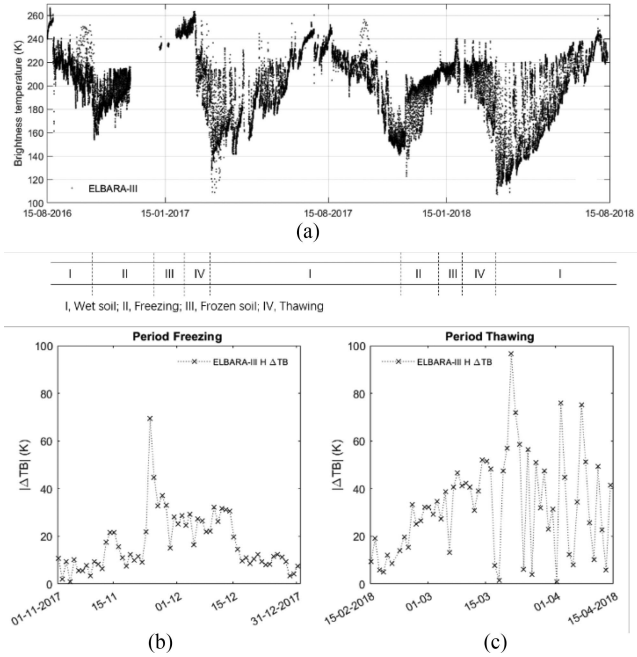

Fig. 2. (a) T_B time-series observed by ELBARA-III (small dots) with an incidence angle of 40° in H-polarization. The dataset covers two complete cycles of seasonal freezing and thawing between 2017 and 2018.; $|\Delta T_B|$ for example, (b) period II and (c) period IV observed by ELBARA-III at H-polarizations in 2017–2018.

is more significant than the changes caused by water content variation (ca. 10s K) [43], [44], [45], [46]. Regarding applying *L*-band passive remote sensing of FT states, SMOS, and SMAP have relevant global FT products in which the polarization ratio and single-channel T_B signals are applied [37]. However, there is little information we can retrieve from *L*-band signals rather than the FT states over the frozen soil.

This study analyzes ΔT_B observed by the ground-based *L*-band microwave radiometer ELBARA-III (the ETH *L*-Band radiometer) at Maqu in the Tibetan Plateau [16]. Then, it develops a brightness temperature inferred freezing front (BT-FF) model that can retrieve the freezing front depth ($z_{\rm ff}$) from ΔT_B. $z_{\rm ff}$ is defined as the annual FT dynamics front in the soil profile. The rest of this article is organized as follows. Section II-A introduces the tower-based *L*-band radiometer and the Maqu Experiment; Section II-B describes the soil temperature simulation results from the land surface model and analyzes the impact of the FT transitions occurring on the soil surface or in deeper layers; Section II-C derives the relation between ΔT_B and $z_{\rm ff}$ from microwave transfer model [47] and Stefan's Equation [48]. Section III validates the BT-FF model with T_B observations and the modeled soil temperature data. Finally, Section IV concludes this article.

II. Observations and Methodology

The data to validate the BT-FF model contains T_B observation from ELBARA-III and modeled soil temperature data from a land surface model named simultaneous transfer of energy, mass, and momentum in unsaturated soil with FT (STEMMUS-FT).

A. T_B Observations

The Maqu monitoring network was established in 2008 in the eastern part of the Tibetan plateau [49], [50], [51] [see Fig. 1(a)]. The Yellow River bounds the network at its eastern and northern brinks, and its landscape is covered by meadow interspersed by a few trees or bushes. Its elevation is about 3300 m, and the rainy summer period caused by the East Asia Summer Monsoon is relatively short (July/August). On an annual scale, the wintertime can last for more than half a year, from October to March. Since December 2015, the *L*-band (1.41 GHz) radiometer ELBARA-III installed at Maqu's central station observes the typical meadow vegetation with a 40 m × 25 m footprint at incidence angles from 40° to 70° varying at 5° steps [see Fig. 1(b)]. In this study, we analyze the observations at 40° to stay consistent with the SMAP observations and focus on a two-year period from August 2016 to August 2018 [see Fig. 2(a)]. The period contains two complete annual FT cycles and the freezing and thawing periods, respectively.

Furtherly, we separate the observations into periods according to daily soil temperature at 2.5 cm ($T_{2.5\ \rm cm}$) characterized by unfrozen soil (I, a minimum of $T_{2.5\ \rm cm} > 0$ °C), freezing soil (II, from I to III), frozen soil (III, a maximum of $T_{2.5\ \rm cm} < 0$ °C), and thawing soil (IV, from III to I) periods [the vertical dashed lines in Fig. 2(a)]. A lot of studies done with these dataset has proved that 2.5 cm is the most effective layer sensed by the radiometer [23], [33]. Even though the sensing depth varies for the frozen soil, 2.5 cm can be taken as an average and representative depth in this study.

Generally, ΔT_B during Period I is dominated by rainfall and evaporation via changing θ and T. T_B has higher values in the early afternoon and lowest values in the morning, and T_B varies by about 10 K daily, respectively. In contrast, ΔT_B is minimal during Period III because the high microwave penetration depth returns T_B characteristic for a relatively large soil column; here, ΔT_B stays less than 5 K. For Period II [see Fig. 2(b)] and IV [see Fig. 2(c)], ΔT_B signals are more complicated to

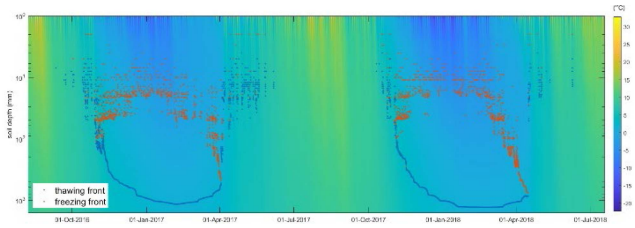

Fig. 3. Soil temperature profile evolution simulated by STEMMUS-FT and the daily thawing front (thawed-up-frozen-down, red dots) and annual freezing front (frozen-up-thawed-down, blue dots) as inferred from soil temperatures.

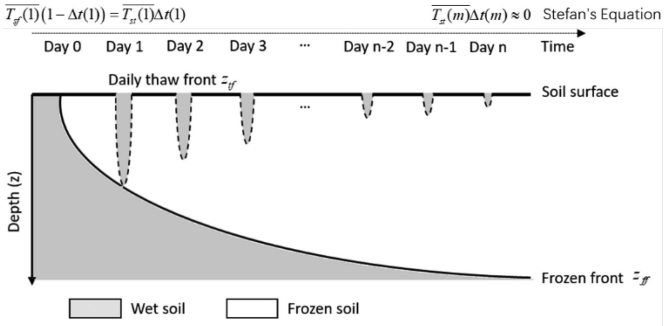

Fig. 4. Illustration of the freezing process assumptions in the BT-FF model. z_{ff} is the freezing front, reflecting the annual FT state cycle, and z_{tf} is the daily thawing front caused, e.g., by radiative heating during daytime. Symbol m is the total lasting days of the annual freezing process, i.e., the last day of period II.

interpret. The large $|\Delta T_B|$ cannot be fully explained by either daily soil temperature or penetration depth variations. As shown in Fig. 2(b) and (c), $|\Delta T_B|$ can reach 20 K daily. Only Subdaily FT transitions can explain it, e.g., the radiative heating over the daytime thaws the upper frozen soil, which means unfrozen soil appears at the surface [39]. Besides, in Period IV, the ponded water can drastically reduce the soil surface emissivity and penetration depth, mixing the signal of an FT transition and a water/ice phase transition.

B. STEMMUS-FT and Soil Temperature Data

With a 1 cm resolution in the vertical direction achieved by STEMMUS-FT, we can capture the daily thawing process caused by the daytime heating effect. The minimum vertical resolution that can be done by measurement is 2.5 cm, which cannot satisfy the requirements of this study. Furthermore, the sensors using TDR methods are hard to be installed over the soil surface where the depth is shallower than 2.5 cm due to their cylindrical sensing area.

STEMMUS-FT [52] is a land model coded in MATLAB with extra modules based on STEMMUS [53], enhancing its capacity in FT simulations. In STEMMUS-FT, frozen soil is the thermal equilibrium system of soil grains, liquid water, ice, water vapor, and dry air [54], [55], [56], [57], [58]. The dynamics of the individual soil components, including soil\ice\water\vaper, interacting with each other were explicitly considered and resolved. Soil water and heat transfer are tightly coupled and realized by solving the equations of water conservation and energy conservation. Additional details on the STEMMUS(-FT) can be found in [59], [60].

Fig. 3 shows STEMMUS-FT's T simulations at Maqu, identifying freezing soil depth (z_{ff}) and thawing soil depth (z_{tf}). z_{ff} is defined as T at z_{ff}, where $T_{\mathrm{upper\ layer}} < 0\ ^{\circ}\mathrm{C} < T_{\mathrm{lower\ layer}}$ and reversely for z_{tf}, where $T_{\mathrm{upper\ layer}} > 0\ ^{\circ}\mathrm{C} > T_{\mathrm{lower\ layer}}$. During Period II, the amplitude of z_{tf} due to the daily FT cycles is large, with a maximum of about 10 cm from the surface to the deeper layer. In Fig. 3, the amplitude of z_{tf} corresponds to the development of the z_{ff}. For instance, the daily freezing and thawing cycles were damped in Period II, and the growth of z_{ff} was decreased in Period III. In Period IV, z_{tf} goes deeper rapidly until the end of z_{ff} in about April.

Compared with Fig. 2, $|\Delta T_B|$ changes visually correlate well with the daily z_{tf} changes affected by T variations between 0 and 0.2 m in Fig. 3. When the surface soil freezes at night, the deeper soil layers—frozen or thawed—will contribute to T_B, but with a weaker attenuating effect from the frozen soil above than at the daytime. In Figs. 2 and 3, T_B does not change much at night, even when the soil profile shows a frozen-moist (downwards, hereafter) structure. In contrast, daytime thawing of the surface soil significantly reduces the penetration depth, leading to a moist-frozen-moist structure in the soil profile. Especially during Periods II and IV, this moist-frozen-moist structure appears shortly during the daytime and completely disappears at night. Besides the FT state vertical structures, another reason that may cause $|\Delta T_B|$ is open water due to melted snow or ice. It is noted that during Period IV, the frozen soil layer below the surface impedes draining and increases the residual water at the surface. Open surface water cannot appear in period frozen since snow is much more common than rainfall.

C. Derivation of the BT-FF Model

The proposed BT-FF model covers both the annual FT cycle regarding z_{ff} and the daily FT processes, leading to ΔT_B via z_{tf}. The BT-FF model is based on the 0th-order microwave transfer model (see Section II-C-1) and relates ΔT_B between two observation times within 24 h to the respective change of z_{tf} (and $z_{\mathrm{tf}}(n)$ for z_{tf} on the nth day after the beginning of the yearly FT cycles). We estimate the temporal evolution of z_{ff} from $z_{\mathrm{tf}}/z_{\mathrm{tf}}(n)$ via Stefan's equation (see Section II-C-2). To clarify, we refer $z_{\mathrm{tf}}/z_{\mathrm{tf}}(n)$ to daily FT cycles while z_{ff} refers to annual FT dynamics, e.g., during Period II (See symbols in the Appendix).

1) 0th-Order Microwave Transfer Model: The 0th-order incoherent model extensively used in passive microwave remote sensing of soil moisture is formulated as

$$T_B = ET_{\mathrm{eff}} \tag{1}$$

where T_B is the observed brightness temperature in K, E is the soil slab's emissivity contributing to T_B, and T_{eff} is the so-called effective temperature of the soil slab. E depends on θ and other factors affecting the dielectric constant of a soil column. T_{eff} relies on the dielectric constant as well. The penetration (e-folding) depth—as a measure of the soil slab depth mainly contributing to T_B—depends on the dielectric constant profile and can reach a depth of meters down in extremely dry but also

frozen soil at the *L*-band. For instance, Fig. 3 shows that in the first few days of Period II, the soil is frozen down to about 20–40 cm, and the soil below the frozen layer does not contribute significantly to the observed T_B (e.g., a short period before z_{tf} grows).

We further assume that both T and dielectric constant are vertically constant in the frozen layer; then (1) can be rewritten as

$$T_B = E_f T \tag{2}$$

with T the frozen layer's temperature and E_f the emissivity of the upper thawed soil layer. According to the red dots in Fig. 3, a thin upper soil layer (less than 20 cm) has thawed at 6 pm due to the daytime solar heating, giving rise to a thawing front at depth z_{tf}. Considering the optical depth (τ_{tf}) [61], [62] down to z_{tf}, (2) can be formulated as

$$T_B = E_t T(1 - e^{-\tau_{\mathrm{tf}}}) + E_f T e^{-\tau_{\mathrm{tf}}} \tag{3}$$

where E_t is the emissivity of the upper thawed soil layer. By $e^{-\tau_{\mathrm{tf}}}$, the opacity stands for reflectivity/scattering of the internal/upper soil layer. We further assume that the temperature of the ice-water mixture is always close to 0°C, which is the normal case during freezing and thawing, then ΔT_B between morning and late afternoon is

$$\begin{aligned}\Delta T_B &= E_t T(1 - e^{-\tau_{\mathrm{tf}}}) + E_f T e^{-\tau_{\mathrm{tf}}} - E_f T \\ &= E_t T(1 - e^{-\tau_{\mathrm{tf}}}) - E_f T\left(1 - e^{-\tau_{\mathrm{tf}}}\right) \\ &= (E_t - E_f)\, T\left(1 - e^{-\tau_{\mathrm{tf}}}\right). \end{aligned} \tag{4}$$

τ_{tf} can be transferred to the corresponding z_{tf} [62], [63] is given by

$$\tau_{\mathrm{tf}} = \frac{2\pi \varepsilon''_t}{\lambda \sqrt{\varepsilon'_t}} z_{\mathrm{tf}} \tag{5}$$

with ε'_t and ε''_t the real and imaginary part of the dielectric constant of the thawed soil calculated from [64]. With $a = (E_t - E_f)T$ and $b_t = \frac{\lambda\sqrt{\varepsilon'_t}}{2\pi\varepsilon''_t}$ the penetration or e-folding depth in the thawed soil, we get

$$z_{\mathrm{tf}} = -b_t \ln\left(1 - \frac{\Delta T_B}{a}\right) \tag{6}$$

which relates ΔT_B to z_{tf}. Thus, we can infer z_{tf} with given E_t and E_f. z_{tf} is quantified by the simulation result from STEMMUS-FT.

2) Stefan's Equation: Both ΔT_B and z_{tf} are caused by surface thawing and refreezing (see Section II-C-1), and they vary daily. The z_{ff} propagation (see Section II-C-2) evolves at an annual scale. We use Stefan's equation [48], [65], [66] to model both the propagation of z_{tf} and z_{ff} (here, both fronts are indicated by z_i), based on the soil skin temperature time series via

$$z_j = \sqrt{c_j I(t)} \tag{7}$$

where Subscript *j* stands for either thawed (Subscript *t*) or frozen soil (Subscript *f*), $c_j = \frac{2k_j}{L\theta\rho}$ ($[c_i] = \mathrm{m}^2\ ^\circ\mathrm{C}^{-1}\mathrm{s}^{-1}$) with k_j the thermal conductivity of frozen or thawed soil ($[k_j] = \mathrm{W\ m}^{-1}\ ^\circ\mathrm{C}^{-1}$) that can be considered as a pair of constants, L the latent heat for water ($3.34 \times 10^5\ \mathrm{J\ kg}^{-1}$), θ is soil moisture when the annual freezing cycle starts in the unit of $\mathrm{m}^3\mathrm{m}^{-3}$), ρ the density of ice ($[\rho] = \mathrm{kg\ m}^{-3}$), and $I = \int_{t_1}^{t_2} |T_s(t)|dt$ the temporal integral of the soil skin temperature (T_s) in °C during freezing ($T_s < 0$ °C) or thawing ($T_s > 0$ °C) between the Time t_1 and t_2, with t_1/t_2 being the beginning/ending of either the annual FT cycle or the daily FT cycle. For a specific day in Period II, T_s might increase above 0 °C, leading to the surface soil ice thawing over time $\Delta t = t_2 - t_1$. Accordingly, freezing ($T_s < 0$ °C) prevails during $t_d - \Delta t$ with t_d the seconds for a day (= 86 400 s). Equation (7) covers annual and diurnal FT cycles that depend on the integral time interval. If the integration stands for the annual cycle, we can obtain z_{ff} by (7); otherwise, z_{tf} is calculated by considering the daytime radiation heating effect over the frozen soil. Thus, we get z_{ff} and z_{tf} on day *n* after the start of Period II, $z_{\mathrm{ff}}(n)$ and $z_{\mathrm{tf}}(n)$, respectively, following (7) as

$$\begin{cases} z_{\mathrm{tf}}(n) = \sqrt{c_t \overline{T_{\mathrm{st}}(n)} \Delta t(n)} \\ z_{\mathrm{ff}}(n) = \sqrt{c_f \overline{T_{\mathrm{sf}}(n)} \Delta t_f(n)} \\ \quad = \sqrt{\sum_{i=1}^{n} c_f \overline{T_{\mathrm{sf}}(i)}\,(t_d - \Delta t(i))} \end{cases} \tag{8}$$

where $\overline{T_{\mathrm{st}}(n)}$ is average T_s at daily thawing time on Day *n*, $\Delta t(n)$ the duration of the thawing on *n*th day, $\overline{T_{\mathrm{sf}}(i)}$ the average soil skin temperature during daily freezing lasting for $t_d - \Delta t(i)$ seconds on Day *i*, $\overline{T_{\mathrm{sf}}(n)}$ is the average skin temperature during freezing from day 1 to day *n*, and $\Delta t_f(n) = \sum_{i=1}^{n} (t_d - \Delta t(i))$ the overall freezing duration from day 1 to day *n*. $z_{\mathrm{tf}}(n)$ and $z_{\mathrm{ff}}(n)$ on day *n* are related via

$$\begin{aligned}\frac{z_{\mathrm{tf}}(n)}{z_{\mathrm{ff}}(n)} &= \frac{\sqrt{c_t \overline{T_{\mathrm{st}}(n)} \Delta t(n)}}{\sqrt{\sum_{i=1}^{n} c_f \overline{T_{\mathrm{sf}}(i)}\,(t_d - \Delta t(i))}} \\ &= \sqrt{\frac{c_t}{c_f}} \frac{\sqrt{\overline{T_{\mathrm{st}}(n)} \Delta t(n)}}{\sqrt{\sum_{i=1}^{n} \overline{T_{\mathrm{sf}}(i)}\,(t_d - \Delta t(i))}} \end{aligned} \tag{9}$$

with $\sqrt{\frac{c_t}{c_f}}$ assumed constant during the FT cycles since k_i and θ are assumed to be constant. The average soil skin temperature on any day *n* ($\overline{T_s(n)}$) and its average until and including day *n* is given by

$$\overline{T_s(n)} = \frac{\overline{T_{\mathrm{sf}}(n)}\,(t_d - \Delta t(n))}{t_d} + \frac{\overline{T_{\mathrm{st}}(n)} \Delta t(n)}{t_d}. \tag{10}$$

Equation (10) means $\overline{T_s(n)}$ can be separated into freezing (i.e., $\frac{\overline{T_{\mathrm{sf}}(n)}(t_d - \Delta t(n))}{t_d}$) and thawing process (i.e., $\frac{\overline{T_{\mathrm{st}}(n)} \Delta t(n)}{t_d}$), which can be used in (7). For instance, if $\Delta t(n) = \frac{1}{2} t_d$ and $\overline{T_{\mathrm{sf}}(n)} = -\overline{T_{\mathrm{st}}(n)}$ on the first day ($n = 1$), then $T_{s1} = \overline{T_{\mathrm{sf}}(n)} + \overline{T_{\mathrm{st}}(n)} = 0$ °C.

The *T* propagation with time and depth can be described as a sine wave by using a Fourier-serie [67], [68] as

$$T(z_a, t) = \left\{ \begin{array}{l} \overline{T} + A \exp\left[-(z_a - z_b)\sqrt{\omega/2k_l}\right] * \\ \sin\left\{\omega t - \phi\left[-(z_a - z_b)\sqrt{\omega/2k_l}\right]\right\} \end{array} \right\} \tag{11}$$

where z_a/z_b is the vertical coordinate positive downward, t is the time; $\overline{T}$ is the temporal average of the soil temperature, and A is half of the difference between the maximum and minimum at z_b; $\omega = \frac{2\pi}{t_d} = \frac{2\pi}{86\,400\ \mathrm{s}}$ is the angular velocity of the Earth's rotation; ϕ is the initial phases of the soil temperature at depth z_b; and $1/\sqrt{\omega/2k_i}$ is the damping depth of the diurnal temperature wave. Thus, z_a-$z_b = 0$ and $z_a = 0$. The freezing period starts from daily $\overline{T_s} = 0$ °C, so we get $\overline{T} = \overline{T_s} = 0$ °C. We assume T_s time-series whose maximum/minimum is $T_s(1)$/$-T_s(1)$ on the day $n = 1$, then $A = T_s(1)$. In this case, a surface soil temperature time series without trend can be simplified as

$$T_s(t) = T_s(1)\sin(\omega t). \tag{12}$$

To further simply (11), the freezing period ends when the daily maximum $T_s = 0$. Equation (12) is expented with a linear trend to mimic the daily T_s variation during Period II as shown in [69] and [70]

$$\begin{aligned} T_s(t) &= T_s(1)\sin(\omega t) - 2T_s(1)\frac{t}{mt_d} \\ &= T_s(1)\left[\sin(\omega t) - 2\frac{t}{mt_d}\right] \end{aligned} \tag{13}$$

where m is the lasting days of Period II (i.e., the total number of days starting from daily $\overline{T_s} = 0$ to the ending at daily maximum $T_s = 0$), and t is the accumulated seconds after Day $i = 1$. Equation (13) represents a T_s time-series whose maximum/minimum is $T_s(1)$/$-T_s(1)$ on the day $n = 1$ and gets below 0 °C on the day $i = n$. Then, (13) is written as

$$\frac{T_s(t)}{T_s(1)} = \sin(\omega t) - 2\frac{t}{mt_d} \tag{14}$$

and (10) is written as

$$\frac{\overline{T_s(n)}}{T_s(1)}t_d = \frac{\overline{T_{\mathrm{sf}}(n)}}{T_s(1)}(t_d - \Delta t(n)) + \frac{\overline{T_{\mathrm{st}}(n)}}{T_s(1)}\Delta t_i. \tag{15}$$

$\overline{T_s(n)}$, $\overline{T_{\mathrm{sf}}(n)}$, $\overline{T_{\mathrm{st}}(n)}$ are defined by $\overline{T_x} = \frac{1}{\Delta t}\int T_s(t)dt$, where x can be i/sf/st or others depending on the averaging time interval for T. Thus, in the BT-FF model, $\overline{T_s(n)}$ decreases from 0 °C ($i = 1$) to $-T_s(1)$ ($n = m$), $\overline{T_{\mathrm{st}}(n)}$ decreases from $T_s(1)$ to 0 °C ($n = m$), and $\overline{T_{\mathrm{sf}}(n)}$ decreases from $T_s(1)$ to $-2T_s(1)$ ($n = m$).

By considering $T_s(1)$, (9) can be rewritten as

$$\frac{z_{\mathrm{tf}}(n)}{z_{\mathrm{ff}}(n)} = \sqrt{\frac{c_t}{c_f}}\left[\sqrt{\frac{\overline{T_{\mathrm{st}}(n)}}{T_s(1)}\Delta t(n)}\Big/\sqrt{\sum_{i=1}^{n}\frac{\overline{T_{\mathrm{sf}}(i)}}{T_s(1)}(t_d - \Delta t(i))}\right]. \tag{16}$$

Since $T_s(1)$ is a constant, Fig. 5(a) focuses on the $[\sin(\omega t) - 2\frac{t}{mt_d}]$ part to infer the ratio of $\frac{z_{\mathrm{tf}}(n)}{z_{\mathrm{ff}}(n)}$ in (16). Fig. 5(a) illustrates the $[\sin(\omega t) - 2\frac{t}{mt_d}]$ time series with $m = 5$ days, $m = 25$ days, and $m = 100$ days. The pink area for the nth day is $\frac{\overline{T_{\mathrm{st}}(n)}}{T_s(1)}\Delta t(n)$, while the sum of the blue area from first to nth day is $\sum_{i=1}^{n}\frac{\overline{T_{\mathrm{sf}}(i)}}{T_s(1)}(t_d - \Delta t(i))$. Fig. 5(b) shows the slope

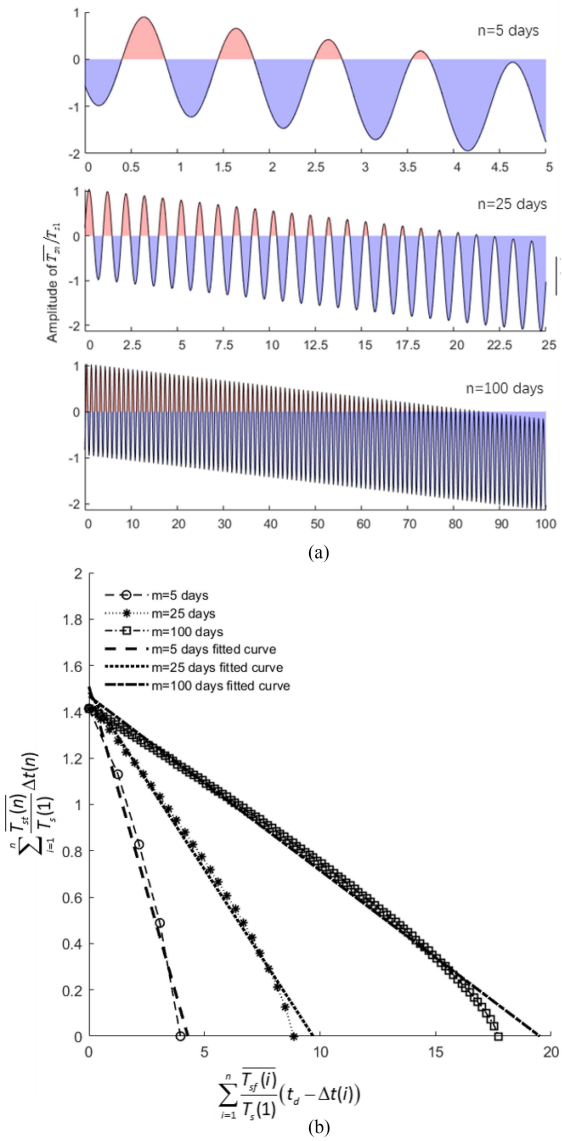

Fig. 5. (a) Time series of a sine wave to mimic the daily variation of $\overline{T_s(n)}/T_s(1)$ discussed in (16) by assuming a freezing process lasting for 5/25/100 days (left). (b) Illustration of $\sqrt{\frac{\overline{T_{\mathrm{st}}(n)}}{T_s(1)}\Delta t(n)}/\sqrt{\sum_{i=1}^{n}\frac{\overline{T_{\mathrm{sf}}(i)}}{T_s(1)}(t_d - \Delta t(i))}$ ratio by the $\overline{T_s(n)}/T_s(1)$ sinewave model in (a).

of $\sqrt{\frac{\overline{T_{\mathrm{st}}(n)}}{T_s(1)}\Delta t(n)}$ over $\sqrt{\sum_{i=1}^{n}\frac{\overline{T_{\mathrm{sf}}(i)}}{T_s(1)}(t_d - \Delta t(i))}$ when $m = 5$ days, $m = 25$ days, and $m = 100$ days. Generally, the slope can be simplified as a constant that depends on m, i.e., how many days Period II can last.

Thus, the hypothesis that $z_{\mathrm{ff}}(n)$ and $z_{\mathrm{tf}}(n)$ in (16) and (6) are nearly linear related is solid. We now propose a linear regression function

$$z_{\mathrm{tf}}(n) = \alpha(m)z_{\mathrm{ff}}(n) + \beta(m). \tag{17}$$

$\alpha(m)$ and $\beta(m)$ can be identified by linear fitting of $z_{\mathrm{ff}}(n)$ and $z_{\mathrm{tf}}(n)$ from STEMMUS-FT simulation results [see Fig. 5(b)]. It is seen that the error of linear approximation is larger when the vertical coordinate is smaller. The relative error is about 10%

for all m values. In other words, the shorter Period II for a given site, the smaller $\alpha(m)$ ($\alpha(m) < 0$). Equation (17) is adopted in the following to infer $z_{\rm ff}(n)$ from $z_{\rm tf}(n)$. By using (17), the linear curve must fit for the first day in Period II when the L-band can detect the daily FT cycles, which means $z_{\rm ff}(1) \approx z_{\rm tf}(1)$, i.e.,

$$(1-\alpha(m))\, z_{\rm ff}(1) = \beta(m). \tag{18}$$

For m days of the L-band T_B detectable in Period II, i.e., the daily maximum $T_s < 0$ °C, we get $z_{\rm tf}(m) = 0$. Then

$$\alpha(m) z_{\rm ff}(m) + \beta(m) = 0. \tag{19}$$

By considering (18) and (19), we get

$$\begin{cases} \alpha(m) = \frac{-z_{\rm ff}(1)}{z_{\rm ff}(m) - z_{\rm ff}(1)} \\ \beta(m) = \frac{z_{\rm ff}(1) z_{\rm ff}(m)}{z_{\rm ff}(m) - z_{\rm ff}(1)} \end{cases}. \tag{20}$$

3) BT-FF Model: With the linear relation given by (17) and its appropriateness demonstrated in Fig. 5(b), we can substitute (6) into (17), we get the BT-FF model as

$$z_{\rm ff}(n) = -\frac{1}{\alpha(m)} \left[b_t \ln\left(1 - \frac{\Delta T_B}{a}\right) + \beta(m) \right]. \tag{21}$$

Equation (21) relates the ΔT_B with the annual frozen front $z_{\rm ff}(n)$. As mentioned above, we assumed the soil moisture content of thawed soil in the annual freezing process does not change with depth and time, which leads to b_t = Constant. Thus, Parameters a, b_t, are constant in the BT-FF model.

III. Results

Equation (6) explains the relationship between $z_{\rm tf}$ and ΔT_B in theory. The parameters, i.e., a and b_t, are defined explicitly. Thus, a and b_t can be estimated with the dielectric constant. In detail, a dielectric constant model requires only clay, sand fraction, soil moisture (soil water content after thawing), soil temperature, and some optional inputs. The clay/sand fractions are constant for a fixed location, and T, if not crossing the freezing point of water, has less impact on the dielectric constant than θ and the FT states. According to [71], the clay fraction over the top is 9.85%, and the sand fraction is 26.95%. $\theta = 0.275$ cm^3/cm^3 is the STEMMUS simulated soil moisture content at the moment when Period II started in 2017. Fig. 6(a) and (b) illustrates the variation of a/b_t along with θ using the Wu's model for frozen soil to caculate E_f [64] and the Mironov's model for unfrozen soil' E_t, ε'_t, and ε''_t [72].

Parameter a ranges from -20 K to 100 K while soil moisture increases from 0.05 cm^3/cm^3 to 0.6 cm^3/cm^3 [see Fig. 6(a)]. The negative a means the unfrozen arid soil has smaller emissivity than after frozen one. Parameter a also means that the maximum ΔT_B can be caused by the FT transition so that the higher θ leads to larger ΔT_B. It should be noted that Parameter a also depends on the polarization besides θ, but the difference between H-pol and V-pol is less than 10 K in Fig. 6(a). On the other hand, b_t decreases with soil moisture exponentially. A certain $z_{\rm tf}$ means the soil optical depth is reduced while freezing.

Equation (16) contains the variables c_t/c_f for the heat capacity when the soil bulk is unfrozen/frozen. For a site like Maqu, c_t/c_f could be considered constant once the soil moisture (or soil water content in either liquid or solid) is fixed. For Maqu, $\sqrt{\frac{c_t}{c_f}} = 0.76$ is adapted here. Thus, Parameter $\alpha(m)$ is determined by the lasting days of Period II (n). For Parameter $\beta(m)$, it depends on n as well as the amplitude of the soil skin temperature time-series (i.e., $T_s(1)$). Fig. 7(a) shows the theoretical values of $\alpha(m)$ along with the freezing days according to (20). The increasing α_n means the $z_{\rm ff}$ grows more slowly if the freezing process lasts longer. In Figs. 2(a) and 3, the freezing process at Maqu in the winter of 2016–2017 and 2017–2018 lasts about 75 days from November 1st to January 15th. Thus, $\alpha(75)$ is estimated as $\alpha(75) = -0.066$. Fig. 7(b) is $\beta(75)$ estimations by setting $T_s(1)$ in [1 k, 60 k] while assuming the freezing days is 75. At Maqu, $T_s(1) =$ 30 K is marked according to the soil temperature simulations in Fig. 3.

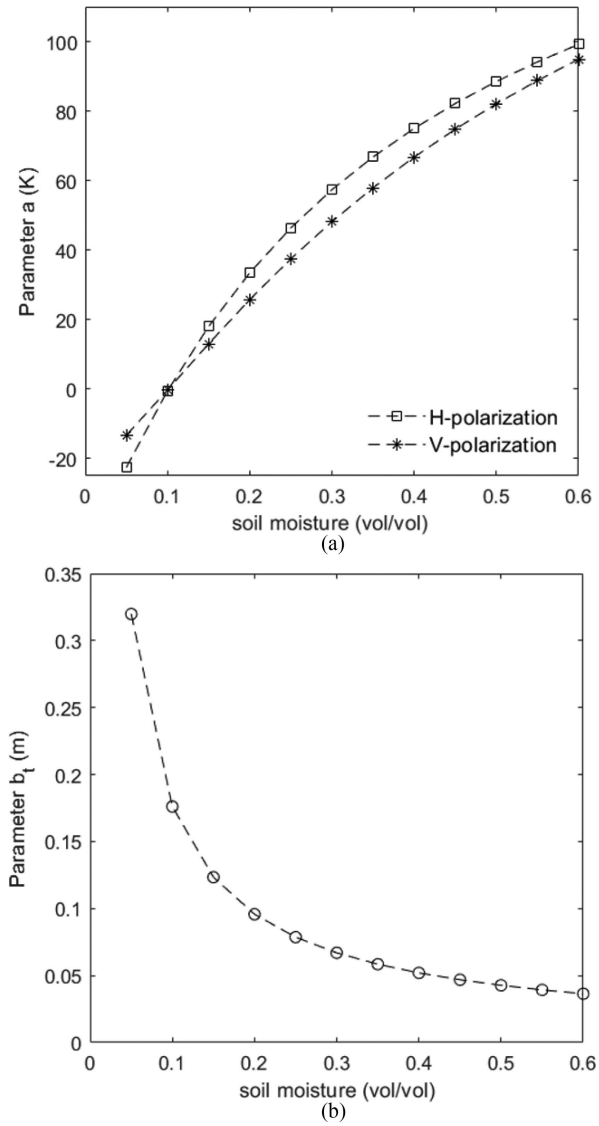

Fig. 6. Estimation of parameter a (a) parameter b_t (b) according to soil water/ice content in (6).

While Figs. 6 and 7 give a full scale of $a/b_t/\alpha(m)$ /$\beta(m)$ estimates, we can also get these parameters from T_B and STEMMUS-FT's simulations. In Fig. 8, a fitting curve in the form of (6) is used to get a relationship between ΔT_B and $z_{\rm tf}$.

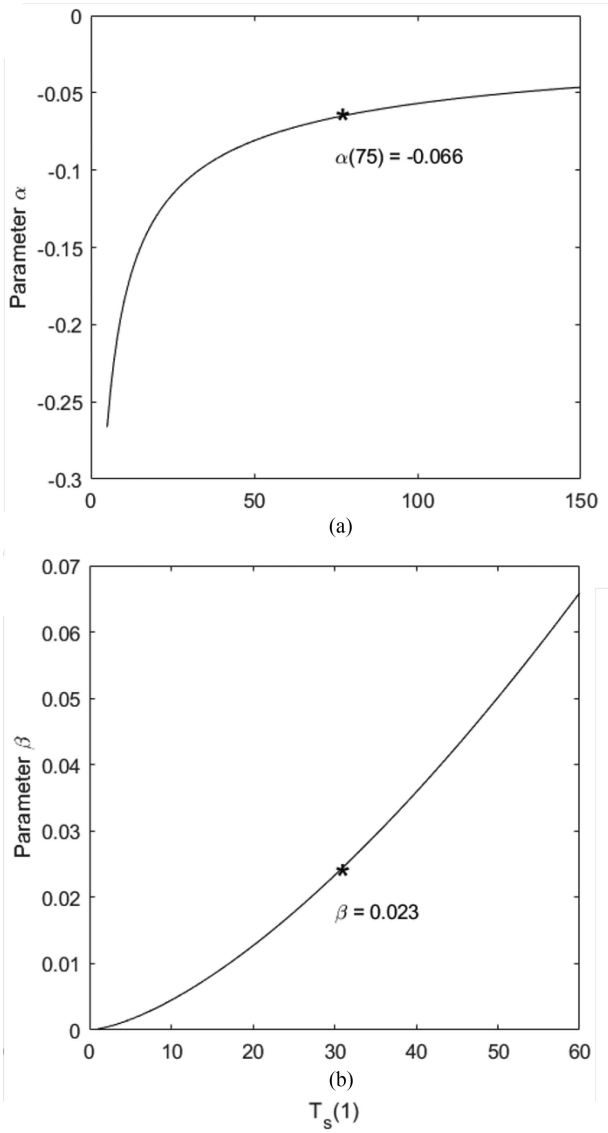

Fig. 7. Estimation of α (left) and β (right) according to $z_{\mathrm{tf}}(n)$ and $z_{\mathrm{ff}}(n)$ in (17) when n increases from 1 to 100 days. $\alpha(75) = -0.066$ and $\beta(75) = 0.023$ are marked out for the Maqu site.

ΔT_B is mainly caused by the temperature difference between 6 A.M. and 6 P.M., and the emissivity changes of F/T status at the upper soil layer, i.e., it can be related to the thawing front. Thus, $a = 68.26$ is derived, which fits the range illustrated in Fig. 6(a). And $b_t = 0.06$ is also obtained, which is equivalent to the value at the θ of about 0.35 $\mathrm{m^3/m^3}$. The regression estimates of a/b_t fit the BT-FF model. In the same way of estimating a/b_t, Fig. 9 shows $\alpha(m)/\beta(m)$ by making a linear regression as shown in (19). It should be noted that the linear regression is made with only the maximum z_{tf} in a day, not all z_{tf} values we get from STEMMUS-FT. We get $\alpha(m) = -0.041$ and $\beta(m) = 0.056$ by averaging 2016–2017 and 2017–2018, which is different from the theoretical estimates in Fig. 7 as $\alpha(m) = -0.066$ and $\beta(m) = 0.023$.

By taking $a/b_t/\alpha(m)/\beta(m)$ estimates from Figs. 6 and 7 into the BT-FF model, we can get z_{ff} and z_{tf} time-series from

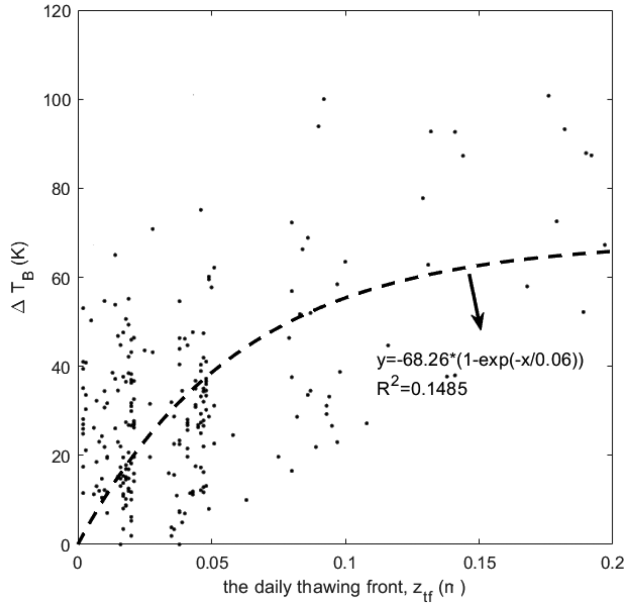

Fig. 8. Relationship between ΔT_B observations and inferred $z_{\mathrm{tf}}(n)$, and its exponential regression ΔT_B versus $z_{\mathrm{tf}}(n)$ relationship as in (6) at Maqu.

ELBARA-III's T_B observations in Period II from 2016 to 2018. The z_{ff} and z_{tf} are compared with z_{ff} and z_{tf} inferred from T simulations in STEMMUS-FT in Fig. 10. Regarding z_{ff}, the RMSE is 12 cm (5–25 cm for 95% confidence). For z_{tf}, the RMSE is 7 cm.

IV. Discussion

Although the BT-FF model has a clear mathematic expression, the uncertainty mostly comes from estimating parameters, i.e., a/b_t from the field measurement and the assumption in derivation.

The BT-FF model is proposed to consider two major assumptions. The first one is that the frozen layer's T and dielectric constant are vertically constant. It is found that the evaporation and draining in the frozen soil are relatively weaker than in the unfrozen soil. Although the vapor diffusion affects the simulation of soil temperature, the effects are relatively small in degrees. The total amount of water removed from the frozen soil in winter is few [46], [73]. This grantee the assumption because the BT-FF model considers only period freezing when the phase change of water cannot be very active due to low daily air temperature.

Regarding soil temperature, the thermal inertia due to radiation heat is consumed as the heat of condensation and sublimation. T at the upper parts of the soil is around 0 °C, while T at the bottom can always be considered constant in the daily time scale [74]. Thus, the second assumption is that the temperature of the ice-water mixture is always close to 0 °C. This assumption is reasonable because the BT-FF model only applies period freezing when a rapid FT transfer happens daily. Regarding the depth interval of z_{tf} (0–10 cm) and the huge thermal inertia of ice-water mixtures, the T gradient must be slight, and its daily average is almost 0 °C.

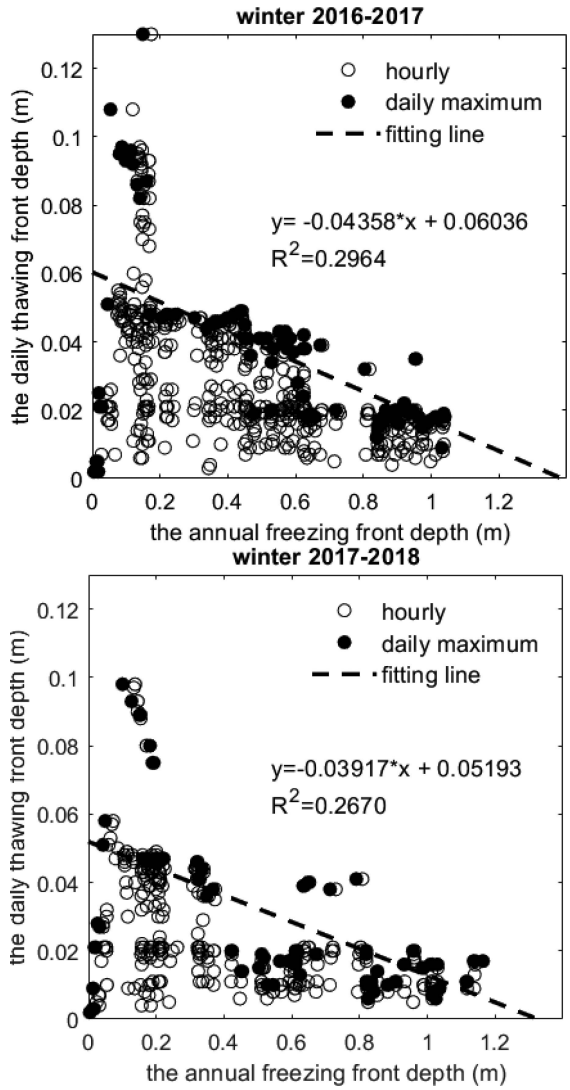

Fig. 9. Linear regression of $z_{\mathrm{tf}}(n) - z_{\mathrm{ff}}(n)$ relationship as in (17) at Maqu.

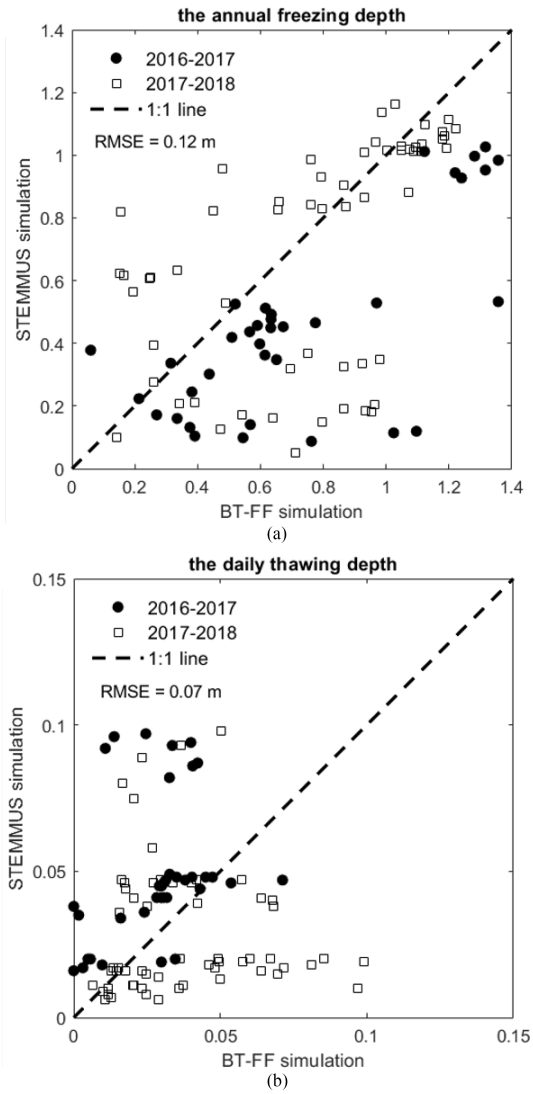

Fig. 10. $z_{\mathrm{ff}}(n)$ prediction from the BT-FF model versus the simulation from STEMMUS-FT.

In contrast, the abovementioned two assumptions are not satisfied in period thawing. The annual freezing and thawing periods have different dynamics impacting ΔT_B. For unfrozen soil, $\boldsymbol{\theta}$ and T profiles change $T_B/\Delta T_B$, especially in the top 10 cm. However, for frozen soil, ΔT_B is dominated by the surface FT state transitions, while $\boldsymbol{\theta}$ and T on the top 10 cm are not crucial for T_B. These conditions simplify the microwave transfer model, leading to the BT-FF model and limiting its application to period freezing.

When it comes to modeling data, applying the BT-FF model at a global scale is not easy. It is challenging to infer z_{ff} even from the land-surface models. For instance, SMOS needs the Hydrology Tiled ECMWF Scheme for Surface Exchanges over Land to provide land surface inputs for retrieval or forward simulations, while SMAP uses the modern-era retrospective analysis for research and applications, Version 2. Both land-surface models have too few layers for computing z_{ff}, and thus, can hardly be used in evaluating the BT-FF model.

V. Conclusion

Previous works lack a theory that can bridge the gap between T_B observation and the FT state of the soil profile during Period II when z_{ff} propagates into deeper soil layers. This theoretical gap hampers the information we can retrieve from the L-band satellite, such as SMAP or SMOS. We propose the BT-FF model, which retrieves the freezing front depth (z_{ff}) from brightness temperature observations in the annual freezing period. The BT-FF model utilizes the Stefan Equation and zeroth-order microwave transfer model to achieve this goal. By taking T_B observations from ELBARA-III and soil temperature simulations from STEMMUS-FT at Maqu, we conclude that ΔT_B between 6 A.M. and 6 P.M. is an optimal pair in retrieving z_{ff}. In the BT-FF model, $\boldsymbol{\theta}$ and T profiles data are unnecessary because we assume $\boldsymbol{\theta}$ and T in deeper layers vary little during Period II.

The concept of soil optical depth (τ) is seldom used in analyzing T_B at L-band. We think τ has advantages over the geometric depth frame (z) in analyzing T_B signals under certain circumstances, such as the freezing/thawing period. The BT-FF

model presented in this study is an application of τ in interpreting the T_B signals at the *L*-band. The BT-FF model is expected to improve our understanding of the freezing/thawing process.

APPENDIX
VARIABLE DEFINITIONS IN SECTION II

α	Fitting parameter (constant) for a specific n.
β	Fitting parameter (constant), $\beta = \max\left(\sqrt{T_{stn}\Delta t_n}\right)$
E	Soil bulk emissivity
E_f	Frozen soil bulk emissivity
E_t	Thawed soil bulk emissivity
ε_t'	The real part of the dielectric constant of thawed soil
ε_t''	Imagery part of the dielectric constant of thawed soil
λ	Wavelengthλ=*21* cm
θ	the volumetric soil moisture content
ρ	the density of ice (kg m^{-3})
τ_{tf}	Soil optical depth of thawed front, $\tau_{tf} = \frac{2\pi\varepsilon_t''}{\lambda\sqrt{\varepsilon_t'}} z_{tf}$
ω	ω=$2\pi/t_d$
Δt	The duration in a day when T_s >0℃
Δt_f	The duration on n days when T_s <0 ℃, $\Delta t_f = \sum_{i=1}^{n}\left(t_d - \Delta t_i\right)$
ΔT_B	temporal T_B changes between two random times within 24
a	aliased as a= $(E_t - E_f)T$
b_t	aliased as $b_t = \frac{\lambda\sqrt{\varepsilon_t'}}{2\pi\varepsilon_t''}$
c_l	aliased as $c_l = \frac{2k_l}{L\theta\rho}$, i.e., C_f for frozen soil and C_t for thawed soil
C_f/ C_t	See c_l
L	the latent heat of fusion for water (3.34×105 J kg-1)
$l(t)$	the temporal integral of the ground skin temperature during freezing/thawing (˚C)
i/n	The i/n days after daily $\overline{T_s}$ =*0*
j	Stands for either thawed (Subscript t) or frozen soil (Subscript f)
m	The total number of days from daily $\overline{T_s}$ =*0 to the maximum of* $\overline{T_s}$ =*0*
k_l	k_l the thermal conductivity of the frozen/thawed soil (W m^{-1} ˚C^{-1})
t_d	Total seconds in a day, 86400s
T	Soil temperature, T=T_{eff} for uniform soil column
T_B	L band brightness temperature
T_{eff}	Soil effective temperature
T_s	the ground skin temperature
T_{s1}	the maximum skin temperature on 1st day
T_{sf}	the average soil skin temperature during $1-\Delta t$, i.e., freezing time
T_{st}	the average soil skin temperature during Δt, i.e., thawing time
z_a/z_b	the vertical coordinate positive downward
z_{ff}	Soil geometric depth of the frozen front
z_i	the depth from the ground surface to the freezing/thawing front, i.e., z_{ff} and z_{tf}
z_{tf}	Soil geometric depth of the thawed front

ACKNOWLEDGMENT

The authors would like to thank the in situ data providers: Xin Wang and Zuoliang Wang, from the Chinese Academy of Sciences.

REFERENCES

[1] C. H. Wang, Z. L. Wang, Y. Kong, F. M. Zhang, K. Yang, and T. J. Zhang, "Most of the Northern hemisphere permafrost remains under climate change," *Sci. Rep.*, vol. 9, Mar. 2019, Art. no. 3295, doi: ARTN 329510.1038/s41598-019-39942-4.

[2] Q. B. Wu and F. J. Niu, "Permafrost changes and engineering stability in Qinghai-Xizang Plateau," *Chin. Sci. Bull.*, vol. 58, no. 10, pp. 1079–1094, Apr. 2013, doi: 10.1007/s11434-012-5587-z.

[3] Y. H. Kerr et al., "The SMOS mission: New tool for monitoring key elements of the global water cycle," *Proc. IEEE*, vol. 98, no. 5, pp. 666–687, May 2010, doi: 10.1109/Jproc.2010.2043032.

[4] K. Rautiainen et al., "L-band radiometer observations of soil processes in boreal and subarctic environments," *IEEE Trans. Geosci. Remote Sens.,* vol. 50, no. 5, pp. 1483–1497, May 2012, doi: 10.1109/Tgrs.2011.2167755.

[5] C. Wang, K. Yang, and F. Zhang, "Impacts of soil freeze–thaw process and snow melting over Tibetan Plateau on asian summer monsoon system: A review and perspective," *Front. Earth Sci.*, vol. 8, 2020, Art. no. 133.

[6] N. V. Smith, S. S. Saatchi, and J. T. Randerson, "Trends in high northern latitude soil freeze and thaw cycles from 1988 to 2002," *J. Geophys. Res.-Atmospheres*, vol. 109, no. D12, Jun. 2004, doi: Artn D12101110.1029/2003jd004472.

[7] G. Y. Niu and Z. L. Yang, "Effects of frozen soil on snowmelt runoff and soil water storage at a continental scale," *J. Hydrometeorol.,* vol. 7, no. 5, pp. 937–952, Oct. 2006, doi: 10.1175/Jhm538.1.

[8] L. Zhang, T. Zhao, L. Jiang, and S. Zhao, "Estimate of phase transition water content in freeze-thaw process using microwave radiometer," *IEEE Trans. Geosci. Remote Sens.,* vol. 48, no. 12, pp. 4248–4255, Dec. 2010, doi: 10.1109/Tgrs.2010.2051158.

[9] L. Y. Yu, Y. J. Zeng, J. Wen, and Z. B. Su, "Liquid-vapor-air flow in the frozen soil," *J. Geophys. Res.-Atmospheres,* vol. 123, no. 14, pp. 7393–7415, Jul. 2018, doi: 10.1029/2018jd028502.

[10] L. Yu, Y. Zeng, J. Wen, and Z. Su, "Liquid-vapor-air flow in the frozen soil," *J. Geoohys. Res.-Atmos.*, vol. 123, pp. 7393–7415, 2018, doi: 10.1029/2018jd028502.

[11] S. Mwangi, Y. J. Zeng, C. Montzka, L. Y. Yu, and Z. B. Su, "Assimilation of cosmic-ray neutron counts for the estimation of soil ice content on the Eastern Tibetan Plateau," *J. Geophysical Res.-Atmospheres*, vol. 125, no. 3, Feb. 2020, doi: ARTN e2019JD03152910.1029/2019JD031529.

[12] M. X. Yang et al., "Diurnal freeze/thaw cycles of the ground surface on the Tibetan Plateau," *Chin. Sci. Bull.,* vol. 52, no. 1, pp. 136–139, Jan. 2007, doi: 10.1007/s11434-007-0004-8.

[13] D. L. Guo, M. X. Yang, and H. J. Wang, "Characteristics of land surface heat and water exchange under different soil freeze/thaw conditions over the central Tibetan Plateau," *Hydrol Process.*, vol. 25, no. 16, pp. 2531–2541, Jul. 2011, doi: 10.1002/hyp.8025.

[14] J. Wen, Z. Wei, S. Lu, S. Chen, Y. Ao, and L. Liang, "Autumn daily characteristics of land surface heat and water exchange over the Loess Plateau mesa in China," *Adv. Atmospheric Sci.,* vol. 24, no. 2, pp. 301–310, Mar. 2007, doi: 10.1007/s00376-007-0301-9.

[15] P. Zhao et al., "The third atmospheric scientific experiment for understanding the earth-atmosphere coupled system over the Tibetan Plateau and its effects," *Bull. Amer. Meteorological Soc.*, vol. 99, no. 4, pp. 757–776, Apr. 2018, doi: 10.1175/Bams-D-16-0050.1.

[16] Z. Su et al., "Multiyear in-situ L-band microwave radiometry of land surface processes on the Tibetan Plateau," *Sci. Data,* vol. 7, no. 1, 2020, Art. no. 317, doi: 10.1038/s41597-020-00657-1.

[17] A. Roy et al., "Spatial variability of L-band brightness temperature during freeze/thaw events over a prairie environment," *Remote Sens.*, vol. 9, no. 9, pp. 894–909, Sep. 2017, doi: ARTN 89410.3390/rs9090894.

[18] A. Roy et al., "Evaluation of spaceborne L-band radiometer measurements for terrestrial freeze/thaw retrievals in Canada," *IEEE J. Sel. Topics Appl. Earth Observ. Remote Sens.*, vol. 8, no. 9, pp. 4442–4459, Sep. 2015, doi: 10.1109/Jstars.2015.2476358.

[19] Y.-A. Liou and A. W. England, "A land-surface process radiobrightness model with coupled heat and moisture transport for freezing soils," *IEEE Trans. Geosci. Remote Sens.*, vol. 36, no. 2, pp. 669–677, Mar. 1998, doi: 10.1109/36.662747.

[20] M. Schwank, M. Stahli, H. Wydler, J. Leuenberger, C. Matzler, and H. Fluhler, "Microwave L-band emission of freezing soil," *IEEE Trans. Geosci. Remote Sens.,* vol. 42, no. 6, pp. 1252–1261, Jun. 2004, doi: 10.1109/Tgrs.2004.825592.

[21] U. Wegmuller, "The effect of freezing and thawing on the microwave signatures of bare soil," *Remote Sens. Environ.*, vol. 33, no. 2, pp. 123–135, Aug. 1990, doi: 10.1016/0034-4257(90)90038-N.

[22] S. M. Bateni, C. Huang, S. A. Margulis, E. Podest, and K. McDonald, "Feasibility of characterizing snowpack and the freeze-thaw state of underlying soil using multifrequency active/passive microwave data," *IEEE Trans. Geosci. Remote Sens.,* vol. 51, no. 7, pp. 4085–4102, Jul. 2013, doi: 10.1109/Tgrs.2012.2229466.

[23] S. Lv, C. Simmer, Y. Zeng, J. Wen, and Z. Su, "The simulation of L-band microwave emission of frozen soil during the thawing period with the community microwave emission model (CMEM)," *J. Remote Sens.*, vol. 2022, 2022, Art. no. 9754341, doi: 10.34133/2022/9754341.

[24] W. Compton and C. Benson, "Living and working in space: A history of skylab," NASA History Office Ser., Sci. Tech. Inform. Branch, Nat. Aeronaut. Space Admin., Washington DC, USA, 1983.

[25] B. Zuerndorfer and A. W. England, "Radiobrightness decision criteria for freeze thaw boundaries," *IEEE Trans. Geosci. Remote Sens.,* vol. 30, no. 1, pp. 89–102, Jan. 1992, doi: 10.1109/36.124219.

[26] J. Judge, J. F. Galantowicz, A. W. England, and P. Dahl, "Freeze/thaw classification for prairie soils using SSM/I radiobrightnesses," *IEEE Trans. Geosci. Remote Sens.,* vol. 35, no. 4, pp. 827–832, Jul. 1997, doi: 10.1109/36.602525.

[27] T. J. Zhao, L. X. Zhang, L. M. Jiang, S. J. Zhao, L. N. Chai, and R. Jin, "A new soil freeze/thaw discriminant algorithm using AMSR-E passive microwave imagery," *Hydrol Process.*, vol. 25, no. 11, pp. 1704–1716, May 2011, doi: 10.1002/hyp.7930.

[28] E. G. Njoku, T. J. Jackson, V. Lakshmi, T. K. Chan, and S. V. Nghiem, "Soil moisture retrieval from AMSR-E," *IEEE Trans. Geosci. Remote Sens.,* vol. 41, no. 2, pp. 215–229, Feb. 2003, doi: 10.1109/tgrs.2002.808243.

[29] J. Y. Du et al., "Inter-calibration of satellite passive microwave land observations from AMSR-E and AMSR2 using overlapping FY3B-MWRI sensor measurements," *Remote Sens.,* vol. 6, no. 9, pp. 8594–8616, Sep. 2014, doi: 10.3390/rs6098594.

[30] W. Wagner et al., "The ASCAT soil moisture product: A review of its specifications, validation results, and emerging applications," *Meteorologische Zeitschrift*, vol. 22, no. 1, pp. 5–33, Feb. 2013, doi: 10.1127/0941-2948/2013/0399.

[31] C. Derksen et al., "Retrieving landscape freeze/thaw state from soil moisture active passive (SNAP) radar and radiometer measurements," *Remote Sens. Environ.*, vol. 194, pp. 48–62, Jun. 2017, doi: 10.1016/j.rse.2017.03.007.

[32] D. Zheng et al., "L-band microwave emission of soil freezesc-thaw process in the third pole environment," *IEEE Trans. Geosci. Remote Sens.*, vol. 55, no. 9, pp. 5324–5338, Sep. 2017.

[33] D. Zheng et al., "Impact of soil permittivity and temperature profile on L-band microwave emission of frozen soil," *IEEE Trans. Geosci. Remote Sens.*, vol. 59, no. 5, pp. 4080–4093, May 2021, doi: 10.1109/TGRS.2020.3024971.

[34] S. Lv, J. Wen, C. Simmer, Y. Zeng, Y. Guo, and Z. Su, "A novel freeze-thaw state detection algorithm based on L-band passive microwave remote sensing," *Remote Sens.*, vol. 14, no. 19, 2022, Art. no. 4747, [Online]. Available: https://www.mdpi.com/2072-4292/14/19/4747

[35] M. Owe, R. de Jeu, and J. Walker, "A methodology for surface soil moisture and vegetation optical depth retrieval using the microwave polarization difference index," *IEEE Trans. Geosci. Remote Sens.,* vol. 39, no. 8, pp. 1643–1654, Aug. 2001, doi: 10.1109/36.942542.

[36] L. Gao, M. Sadeghi, A. Ebtehaj, and J. P. Wigneron, "A temporal polarization ratio algorithm for calibration-free retrieval of soil moisture at L-band," *Remote Sens. Environ.*, vol. 249, Nov. 2020, doi: ARTN 11201910.1016/j.rse.2020.112019.

[37] K. Rautiainen et al., "Detection of soil freezing from L-band passive microwave observations," *Remote Sens. Environ.*, vol. 147, pp. 206–218, 2014.

[38] T. Zhao et al., "Retrievals of soil moisture and vegetation optical depth using a multichannel collaborative algorithm," *Remote Sens. Environ.,* vol. 257, 2021, Art. no. 112321.

[39] S. Lv, C. Simmer, Y. Zeng, Z. Su, and J. Wen, "Impact of profile-averaged soil ice fraction on passive microwave brightness temperature diurnal amplitude variations (DAV) at L-band," *Cold Reg. Sci. Technol.*, vol. 205, 2023, Art. no. 103674, doi: 10.1016/j.coldregions.2022.103674.

[40] M. T. Johnson, J. Ramage, T. J. Troy, and M. J. Brodzik, "Snowmelt detection with calibrated, enhanced-resolution brightness temperatures (CETB) in Colorado Watersheds," *Water Resour. Res.*, vol. 56, no. 1, 2020, Art. no. e2018WR024542, doi: 10.1029/2018WR024542.

[41] J. M. Ramage and B. L. Isacks, "Determination of melt-onset and refreeze timing on southeast Alaskan icefields using SSM/I diurnal amplitude variations," *Ann. Glaciol.,* vol. 34, pp. 391–398, 2002, doi: 10.3189/172756402781817761.

[42] K. A. Semmens, J. Ramage, J. D. Apgar, K. E. Bennett, G. E. Liston, and E. Deeb, "Passive microwave remote sensing of snowmelt and melt-refreeze using diurnal amplitude variations," *Remote Sens. Terr. Water Cycle*, pp. 215–226, 2014.

[43] K. A. Semmens, J. Ramage, J. D. Apgar, K. E. Bennett, G. E. Liston, and E. Deeb, "Passive microwave remote sensing of snowmelt and melt-refreeze using diurnal amplitude variations," *Remote Sens. Terr. Water Cycle*, V. Lakshmi et al., doi: 10.1002/9781118872086.ch13.

[44] V. L. Mironov, Y. H. Kerr, L. G. Kosolapova, I. V. Savin, and K. V. Muzalevskiy, "A temperature-dependent dielectric model for thawed and frozen organic soil at 1.4 GHz," *IEEE J. Sel. Topics Appl. Earth Observ. Remote Sens.,* vol. 8, no. 9, pp. 4470–4477, Sep. 2015, doi: 10.1109/JSTARS.2015.2442295.

[45] V. L. Mironov, K. V. Muzalevskiy, and Z. Ruzicka, "Retrieving profile temperatures in a frozen topsoil near the TFS, Alaska, based on SMOS brightness temperatures at the 1.4-GHz frequency," *IEEE Trans. Geosci. Remote Sens.,* vol. 54, no. 12, pp. 7331–7338, Dec. 2016, doi: 10.1109/Tgrs.2016.2599272.

[46] L. Zhang, J. Shi, Z. Zhang, and K. Zhao, "The estimation of dielectric constant of frozen soil-water mixture at microwave bands," in *Proc. IEEE Int. Geosci. Remote Sens. Symp.*, 2003, vol. 4, pp. 2903–2905, doi: 10.1109/IGARSS.2003.1294626.

[47] E. G. Njoku and J.-A. Kong, "Theory for passive microwave remote-sensing of near-surface soil-moisture," *J. Geophys. Res.,* vol. 82, no. 20, pp. 3108–3118, 1977.

[48] J. Stefan, "Über die theorie der eisbildung, insbesondere über die eisbildung im polarmeere," *Ann. Phys. Chem.*, vol. 278, pp. 269–286, 1891, doi: 10.1002/andp.18912780206.

[49] A. Colliander et al., "An assessment of the differences between spatial resolution and grid size for the SMAP enhanced soil moisture product over homogeneous sites," *Remote Sens. Environ.*, vol. 207, pp. 65–70, Mar. 2018, doi: 10.1016/j.rse.2018.02.006.

[50] Z. Su et al., "The Tibetan Plateau observatory of plateau scale soil moisture and soil temperature (Tibet-Obs) for quantifying uncertainties in coarse resolution satellite and model products," *Hydrol. Earth Syst. Sci.*, vol. 15, no. 7, pp. 2303–2316, 2011, doi: 10.5194/hess-15-2303-2011.

[51] Y. Zeng et al., "Blending satellite observed, model simulated, and in situ measured soil moisture over Tibetan Plateau," *Remote Sens.,* vol. 8, no. 3, 2016, Art. no. 268.

[52] L. Yu, Y. Zeng, and Z. Su, "STEMMUS-UEB v1.0.0: Integrated modelling of snowpack and soil mass and energy transfer with three levels of soil physical process complexities," *Geosci. Model Dev. Discuss.,* pp. 1–42, 2021, doi: 10.5194/gmd-2020-416.

[53] Y. Zeng and Z. Su, "STEMMUS: Simultaneous transfer of engery, mass and momentum in unsaturated soil: ITC-WRS report," Univ. Twente, Fac. Geo-Inform. Earth Observation (ITC): Enschede, The Netherlands, pp. 6161–6164 2013.

[54] P. C. D. Milly, "Moisture and heat transport in hysteretic, inhomogeneous porous media: A matric head-based formulation and a numerical model," *Water Resour. Res.*, vol. 18, no. 3, pp. 489–498, 1982, doi: 10.1029/WR018i003p00489.

[55] L. Yu, Y. Zeng, J. Wen, and Z. Su, "Liquid-vapor-air flow in the frozen soil," *J. Geophysical Res.: Atmospheres,* vol. 123, no. 14, pp. 7393–7415, 2018, doi: 10.1029/2018jd028502.

[56] Y. Zeng, Z. Su, L. Wan, and J. Wen, "A simulation analysis of the advective effect on evaporation using a two-phase heat and mass flow model," *Water Resour. Res.*, vol. 47, no. 10, 2011, Art. no. W10529, doi: 10.1029/2011WR010701.

[57] Y. Zeng, Z. Su, L. Wan, and J. Wen, "Numerical analysis of air-water-heat flow in unsaturated soil: Is it necessary to consider airflow in land surface models?," *J. Geophysical Res.: Atmospheres*, vol. 116, no. D20, 2011, Art. no. D20107, doi: 10.1029/2011JD015835.

[58] Y. J. Zeng and Z. B. Su, *STEMMUS : Simultaneous Transfer of Engery, Mass and Momentum in Unsaturated Soil*. Enschede, The Netherlands: Univ. of Twente, Faculty of Geo-Information and Earth Observation (ITC), 2013.

[59] Y. J. Zeng, Z. B. Su, L. Wan, and J. Wen, "A simulation analysis of the advective effect on evaporation using a two-phase heat and mass flow model," *Water Resour. Res.*, vol. 47, Oct. 2011, Art. no. W10529, doi: 10.1029/2011wr010701.

[60] Y. Zeng, Z. Su, L. Wan, and J. Wen, "Numerical analysis of air-water-heat flow in unsaturated soil: Is it necessary to consider airflow in land surface models?," *J. Geophys. Res.,* vol. 116, Oct. 2011, doi: 10.1029/2011jd015835.

[61] S. Lv, Y. Zeng, Z. Su, and J. Wen, "A closed-form expression of soil temperature sensing depth at L-band," *IEEE Trans. Geosci. Remote Sens.*, vol. 57, no. 7, pp. 4889–4897, Jul. 2019, doi: 10.1109/TGRS.2019.2893687.
[62] S. Lv, Y. Zeng, J. Wen, H. Zhao, and Z. Su, "Estimation of penetration depth from soil effective temperature in microwave radiometry," *Remote Sens.,* vol. 10, no. 4, 2018, Art. no. 519, [Online]. Available: http://www.mdpi.com/2072-4292/10/4/519
[63] T. T. Wilheit, "Radiative-transfer in a plane stratified dielectric," *IEEE Trans. Geosci. Remote Sens.*, vol. 16, no. 2, pp. 138–143, Apr. 1978, doi: 10.1109/tge.1978.294577.
[64] S. Wu, T. Zhao, J. Pan, H. Xue, L. Zhao, and J. Shi, "Improvement in modeling soil dielectric properties during freeze-thaw transitions," *IEEE Geosci. Remote Sens. Lett.*, vol. 19, 2022, Art. no. 2001005, doi: 10.1109/LGRS.2022.3154291.
[65] M.-K. Woo, *Permafrost Hydrology*. Berlin, Germany: Springer, 2012.
[66] T. Wang et al., "Historical and future changes of frozen ground in the upper Yellow River Basin," *Glob. Planet Change*, vol. 162, pp. 199–211, 2018, doi: 10.1016/j.gloplacha.2018.01.009.
[67] G. J. Hu et al., "New Fourier-series-based analytical solution to the conduction-convection equation to calculate soil temperature, determine soil thermal properties, or estimate water flux," *Int. J. Heat Mass Transfer*, vol. 95, pp. 815–823, Apr. 2016, doi: 10.1016/j.ijheatmasstransfer.2015.11.078.
[68] D. Nofziger and J. Wu, *Soil Temperature Variations With Time and Depth. Department of Plant and Soil Sciences*. Stillwater, OK, USA: Oklahoma State Univ., 2005.
[69] Z. Gao, D. H. Lenschow, R. Horton, M. Zhou, L. Wang, and J. Wen, "Comparison of two soil temperature algorithms for a bare ground site on the Loess Plateau in China," *J. Geophysical Res.,* vol. 113, no. D18, 2008, Art. no. D18105, doi: 10.1029/2008jd010285.
[70] Z. Gao, R. Horton, L. Wang, H. Liu, and J. Wen, "An improved force-restore method for soil temperature prediction," *Eur. J. Soil Sci.,* vol. 59, no. 5, pp. 972–981, 2008, doi: 10.1111/j.1365-2389.2008.01060.x.
[71] H. Zhao, Y. Zeng, S. Lv, and Z. Su, "Analysis of soil hydraulic and thermal properties for land surface modelling over the Tibetan Plateau," *Earth Syst. Sci. Data Discuss.*, vol. 10, pp. 1031–1061, 2018, doi: 10.5194/essd-10-1031-2018.
[72] V. L. Mironov and S. V. Fomin, "Temperature dependable microwave dielectric model for moist soils," in *Piers 2009 Beijing: Progess in Electromagnetics Research Symposium, Proceedings I and Ii*, J. A. Kong, Ed., Progress in Electromagnetics Research Symposium. Cambridge, MA, USA: Electromagnetics Academy, 2009, pp. 831–835.
[73] L. Luo et al., "Effects of frozen soil on soil temperature, spring infiltration, and runoff: Results from the PILPS 2(d) experiment at valdai, Russia," *J. Hydrometeorol.,* vol. 4, no. 2, pp. 334–351, Apr. 2003, doi: 10.1175/1525-7541(2003)4<334:Eofsos>2.0.Co;2.
[74] G. Granberg, H. Grip, M. O. Löfvenius, I. Sundh, B. H. Svensson, and M. Nilsson, "A simple model for simulation of water content, soil frost, and soil temperatures in boreal mixed mires," *Water Resour. Res.,* vol. 35, no. 12, pp. 3771–3782, 1999, doi: 10.1029/1999WR900216.

Shaoning Lv received the first Ph.D. degree in atmospheric physics from the Northwest Institute of Eco-Environment and Resources, Chinese Academy of Sciences, Lanzhou, China, in 2014 and the second Ph.D. degree in remote sensing and hydrology from the Water Resources Department, Faculty of Geo-Information Science and Earth Observation, University of Twente, Enschede, The Netherlands, in 2019.

He is currently with the Department of Atmospheric and Oceanic Sciences and Institute of Atmospheric Sciences Fudan University, Shanghai, China. His research interests include passive microwave remote sensing of soil moisture and its application in climate forecast.

Lianyu Yu received the Ph.D. degree in hydrology from the University of Twente, Enschede, The Netherlands, in 2022.

He is currently with the College of Water Resources and Architectural Engineering, Northwest A&F University, Yangling, China. His research interest is to understand the water, heat, and carbon exchange processes across the interfaces "from bedrock to atmosphere," currently with the focus on soil freezing and thawing processes, and groundwater-soil-water-plant-energy interactions.

Yijian Zeng received the Ph.D. degree in hydrology from the University of Twente, Enschede, The Netherlands, in 2012.

He is currently an Assistant Professor with the Water Resources Department, Faculty of Geo-Information Science and Earth Observation, University of Twente. His research interests include land-atmosphere interaction via hydrologic processes and how the interaction affects the climate system, generation of consistent climate data record using multi-source of geo-datasets, physical mechanisms of land surface models, and the application of data assimilation.

Jun Wen received the B.A. degree in meteorology from Peking University, Beijing, China, in 1988, the M.A. degree in meteorology from Lanzhou University, Lanzhou, China, in 1995, and the Ph.D. degree in meteorology from the Chinese Academy of Sciences, Lanzhou, China, in 1999.

He is currently a Professor with the College of Atmospheric Sciences, Chengdu University of Information Technology, Chengdu, China. His research interests include remote sensing and data assimilation, land surface modeling, and climate change.

Clemens Simmer received the B.S. and Ph.D. degrees in meteorology from the University of Cologne, Cologne, Germany, in 1981 and 1983, respectively.

Since 1996, he has been with the Meteorological Institute, University of Bonn, Bonn, Germany, where he is currently the Head of the working group on remote sensing and mesoscale modeling. He is also an expert in coupled modeling of the regional Earth system, model evaluation, data assimilation, satellite and ground-based remote sensing, and regional climate analysis. He is a member of the Center for High-Performance Computing of Terrestrial Systems HPSC TerrSys (www.hpsc-terrsys.de), which helps geoscientists of the Geoverbund ABC/J (alliance of the geosciences within the universities RWTH Aachen, Bonn and Cologne and the Forschungszentrum Jülich) to efficiently use the JSC supercomputers for geoscientific modeling. In the field of ground-based remote sensing, he concentrates on microwave-based active and passive methods with a current focus on precipitation and cloud processes in cooperation with the Jülich Observatory for Cloud Cartography - Core Facility (JOYCE-CF). His efforts in regional climate analysis concentrated in the past on the evaluation of extremes and trends from German and European precipitation observation stations and moved recently to dynamic downscaling of global climate runs.

Zhongbo (Bob) Su received the B.Sc. degree in hydraulic engineering from the Taiyuan University of Technology, Taiyuan, China, in 1984, the M.Sc. degree in hydrological engineering from IHE, Delft, The Netherlands, in 1989, and the Ph.D. degree in civil engineering from the Ruhr University, Bochum, Germany, in 1996.

He is currently a Professor of Spatial Hydrology and Water Resources Management, and Chairman of Faculty of Geo-Information Science and Earth Observation, Department of Water Resources, University of Twente, Enschede, The Netherlands. His current research focuses on remote sensing and numerical modeling of land surface processes and interactions with the atmosphere, Earth observation of water cycle and applications in climate, ecosystem and water resources studies, as well as monitoring food security and water-related disasters.